

Published in final edited form as:

Neuron. 2011 January 27; 69(2): 304–316. doi:10.1016/j.neuron.2010.12.014.

RIM determines Ca²⁺ channel density and vesicle docking at the presynaptic active zone

Yunyun Han¹, Pascal S. Kaeser², Thomas C. Südhof², and Ralf Schneggenburger^{1,*}

¹Laboratory of Synaptic Mechanisms, Brain Mind Institute, École Polytechnique Fédérale de Lausanne (EPFL), 1015 Lausanne, Switzerland ²Department of Molecular and Cellular Physiology and Howard Hughes Medical Institute, Stanford University School of Medicine, Lorry Lokey Stem Cell Research Building, 265 Campus Drive, Stanford, CA 94305-5453

Abstract

At presynaptic active zones, neurotransmitter release is initiated by the opening of voltage-gated Ca²⁺ channels close to docked vesicles. The mechanisms that enrich Ca²⁺ channels at active zones are, however, largely unknown, possibly because of the limited presynaptic accessibility of most synapses. Here, we have established a Cre-lox based conditional knock-out approach at a presynaptically accessible CNS synapse, the calyx of Held, to directly study the functions of RIM proteins. Removal of all RIM1/2 isoforms strongly reduced the presynaptic Ca²⁺ channel density, revealing a new role of RIM proteins in Ca²⁺ channel targeting. Removal of RIMs also reduced the readily-releasable pool, paralleled by a similar reduction of the number of docked vesicles, and the Ca²⁺ channel - vesicle coupling was decreased. Thus, RIM proteins co-ordinately regulate key functions for fast transmitter release: enabling a high presynaptic Ca²⁺ channel density, and vesicle docking at the active zone.

Keywords

transmitter release; presynaptic cytomatrix; synaptic transmission; readily-releasable pool; Ca²⁺ secretion-coupling

Introduction

Action potentials (APs) evoke neurotransmitter release from presynaptic nerve terminals in the process of SNARE-protein - mediated vesicle fusion (Chen and Scheller, 2001; Jahn et al., 2003). Transmitter release is triggered by Ca²⁺ influx through voltage-gated Ca²⁺ channels, and the fast phase of release closely follows the waveform of presynaptic Ca²⁺ current with only a sub-millisecond delay (Sabatini and Regehr, 1996; Borst and Sakmann, 1996). One pre-requisite for the temporal precision of transmitter release is a tight spatial co-localization between docked vesicles and Ca²⁺ channels in the range of a few 10's of nanometers, which enables a short diffusional distance between Ca²⁺ channels and the Ca²⁺ sensor for vesicle fusion (see Neher, 1998 for a review). Thus, there is general agreement

© 2011 Elsevier Inc. All rights reserved.

*corresponding author: (ralf.schneggenburger@epfl.ch).

Publisher's Disclaimer: This is a PDF file of an unedited manuscript that has been accepted for publication. As a service to our customers we are providing this early version of the manuscript. The manuscript will undergo copyediting, typesetting, and review of the resulting proof before it is published in its final citable form. Please note that during the production process errors may be discovered which could affect the content, and all legal disclaimers that apply to the journal pertain.

that Ca^{2+} channels must be enriched within the active zone, as is also suggested from fast Ca^{2+} imaging studies (Llinás et al., 1995; Zenisek et al., 2003) and from initial ultrastructural evidence at CNS synapses (Bucurenciu et al., 2008). However, the molecular mechanisms which enable an enrichment of Ca^{2+} channels at the presynaptic active zone are not well understood.

The presynaptic active zone of synapses consists of a dense accumulation of cytomatrix proteins, some of which, like Munc13, ELKS/CAST and RIM's are localized highly specifically at active zones (Schoch and Gundelfinger, 2006). Amongst these, RIM proteins (Rab3-interacting molecule; Wang et al., 1997) are interesting candidates for scaffolding proteins with possible interactions with voltage-gated Ca^{2+} channels (Coppola et al., 2001; Hibino et al., 2002; Kiyonaka et al., 2007). RIM proteins are encoded by four genes (*Rims1-4*) which drive the expression of seven known RIM isoforms: RIM1 α , 1 β ; RIM2 α , 2 β , 2 γ ; as well as RIM3 γ and RIM4 γ (Wang et al., 2000; Wang and Südhof, 2003; Kaeser et al., 2008). RIM proteins bind to multiple other presynaptic proteins – e.g., Rab3, Munc13's, α -liprins, and RIM-binding proteins (RIM-BPs; Wang et al., 1997; Wang et al., 2000; Betz et al., 2001; Schoch et al., 2002; Dulubova et al., 2005). Genetic removal of RIM1 α in mice, and of the homologous unc10 protein in *C. elegans* has indicated a role of RIMs in transmitter release (Koushika et al., 2001; Schoch et al., 2002; Calakos et al., 2004), as well as in presynaptic forms of long-term plasticity in a synapse-specific way (Castillo et al., 2002). Recent studies proposed multiple potential interactions between RIMs and Ca^{2+} channels. RIM C2-domains were found to bind to L- and P/Q-type Ca^{2+} channels (Coppola et al., 2001). Heterologous expression of RIM1 α in non-neuronal cells reduced the inactivation of co-expressed voltage-gated Ca^{2+} channels via an interaction of the RIM1 C-terminus with Ca^{2+} channel β 4-subunits (Kiyonaka et al., 2007). RIM-BPs have been found to bind to L- and N-type Ca^{2+} -channel α subunits (Hibino et al., 2002). However, the role of RIM proteins for Ca^{2+} entry at the presynaptic nerve terminal has remained unclear, maybe because no previous study eliminated all RIM1/2 isoforms in vertebrates, and because genetically accessible model synapses, like the neuromuscular junctions of *C. elegans* and *Drosophila* and cultured CNS neurons, are not accessible to direct presynaptic recordings.

The calyx of Held in the auditory brainstem is a large synapse accessible to patch-clamp recordings directly at the nerve terminal, which has enabled a uniquely direct control of presynaptic Ca^{2+} for studying the Ca^{2+} regulation of transmitter release (see Schneggenburger and Forsythe, 2006, for a review). However, the usefulness of the calyx preparation has been limited by the fact that many conventional mouse knock-out (KO) models cause perinatal lethality. To overcome this limitation and to allow for a direct study of the presynaptic roles of RIM proteins, we have devised a Cre-lox based conditional KO approach at the calyx of Held synapse, using newly generated RIM1/2 floxed mouse lines (Kaeser et al., *submitted*). We show that the conditional removal of RIM proteins leads to a strong decrease of Ca^{2+} currents in the nerve terminal, providing direct evidence that RIMs enrich Ca^{2+} channels at the presynaptic active zone. RIM1/2 removal also led to a marked reduction in the number of readily-releasable vesicles, which was paralleled by a similar reduction in the number of docked vesicles. Moreover, RIM proteins help to speed the rates of transmitter release both intrinsically and by increasing the coupling of readily-releasable vesicles with Ca^{2+} channels. Thus, RIM proteins coordinate essential functions that ensure fast rates of transmitter release at synapses.

Results

Conditional knock-out of RIM1/2 at the calyx of Held synapse

We wished to investigate the presynaptic function of RIM proteins at the calyx of Held, a large CNS model synapse at which direct measurement of presynaptic Ca^{2+} currents can be

made (see Introduction). However, constitutive RIM1 α /RIM2 α double KO mice die at birth (Schoch et al., 2006) which precludes their analysis at the calyx of Held, and deleting individual RIM isoforms might produce only a weak phenotype because of the functional redundancy among the isoforms (Schoch et al., 2006; Kaeser et al., 2008). We therefore aimed to remove RIM1/2 conditionally at the calyx of Held, using newly produced floxed mouse lines in which the expression of all RIM1 and RIM2 isoforms, including RIM1 β and RIM2 β , can be abolished by expression of Cre-recombinase (Kaeser et al., *submitted*). For this purpose, we searched for a Cre-driver mouse line that expresses Cre-recombinase specifically in the lower auditory brainstem where calyces of Held are located. We found that in Krox20+/Cre mice (Voiculescu et al., 2000), Cre-activity as revealed by a tandem-dimer red fluorescence protein (tdRFP) reporter mouse line (Luche et al., 2007) was present in the lower auditory brainstem as well as in the trigeminal nucleus and some adjacent areas, but importantly, most other areas of the brainstem and CNS were devoid of Cre activity (Fig. S1A). In the ventral cochlear nucleus, which harbors globular bushy cells that generate calyces of Held (see Cant and Benson, 2003, and references therein), a large number of tdRFP-positive neurons were found (Fig. S1B, Fig. 1A). In the MNTB, the target nucleus of calyces of Held, tdRFP was present in postsynaptic neurons, as well as in calyces of Held, which were identified by co-staining with an anti Synaptotagmin2 (Synt2) antibody (Fig. 1B). Thus, Cre activity in Krox20+/Cre mice is present in a neuron population that includes calyx of Held-generating neurons in the cochlear nucleus, which explains the presence of tdRFP-positive large nerve endings in the MNTB.

We crossed the Krox20Cre/+ mice with floxed RIM1/2 mice (Kaeser et al, *submitted*) to generate conditional RIM1/2 double KO mice specific for the auditory brainstem. Due to germline recombination in the Krox20Cre line (Voiculescu et al., 2000), we obtained Cre-positive RIM1/2 lox/ Δ mice (see Experimental Procedures). These mice were viable and fertile, which allowed us to investigate synaptic transmission in brain slice preparations. We will refer to synapses recorded in Cre-positive RIM1/2 lox/ Δ mice as RIM1/2 cDKO synapses (for "conditional double KO"). As a control group, we used Cre-negative, RIM1/2 lox/ Δ littermate mice (see Experimental Procedures). EPSCs evoked by afferent fiber stimulation at calyx of Held synapses in RIM1/2 cDKO mice had amplitudes of only 1.86 ± 1.73 nA ($n = 12$ cells), significantly smaller than in Cre-negative littermate control mice (9.8 ± 4.2 nA; $n = 15$ cells; Fig. 1C, D). The evoked EPSCs also had slightly, but significantly slower rise times (Fig. 1E, F; $p = 0.0038$), reflecting slowed release kinetics which will be analyzed in more detail below (see Figs 4; 5). The amplitude of spontaneous, 'miniature' EPSCs (mEPSCs) was unchanged (Fig. 1G), consistent with a presynaptic transmitter release deficit. Synaptic phenotypes were consistently observed in all synapses studied in RIM1/2 cDKO mice ($n=73$). This indicates that Cre-mediated removal of the RIM proteins was effective, without detectable inhomogeneity across the population of the studied neurons.

RIMs determine presynaptic Ca²⁺ channel density

Having established the conditional removal of all long RIM isoforms at the calyx of Held, we are now in a position to directly study the presynaptic function of RIM1/2 proteins. In current clamp recordings from calyces of Held, presynaptic APs elicited by afferent fiber stimulation were unchanged in RIM1/2 cDKO calyces (Fig. 2), showing that changes in the AP-waveform do not underlie the reduced transmitter release. We next investigated presynaptic Ca²⁺ currents in voltage-clamp recordings of the calyx of Held. Surprisingly, these recordings revealed a strong reduction of the amplitude of Ca²⁺ currents in RIM1/2 cDKO calyces (Fig. 2C). In both genotypes, presynaptic Ca²⁺ currents started to activate at around -20 mV, and the maximal Ca²⁺ current was observed at ~ 0 mV (Fig. 2C, D); however, the maximal Ca²⁺ current was only 500 ± 310 pA ($n = 19$ cells) in RIM1/2 cDKO

calyces, whereas it was 1040 ± 250 pA ($n = 9$) in calyces of control mice (Fig. 2E; $p < 0.001$). Control experiments with Krox20+/Cre mice, and with RIM1lox/RIM2lox mice revealed no significant reduction of the presynaptic Ca^{2+} current (Fig. S2), showing that the reduced Ca^{2+} currents were not caused by the Krox20+/Cre allele, nor by the non-recombined, floxed RIM1/2 alleles. In order to normalize the measured Ca^{2+} current amplitudes for the membrane surface of calyx terminals, we recorded the membrane capacitance C_m of calyces of Held, which was unchanged (12.7 ± 4.0 pF, $n = 19$, and 14.8 ± 3.5 pF, $n = 9$ in RIM1/2 cDKO and control calyces, respectively; $p = 0.16$). The maximal Ca^{2+} current normalized for membrane surface (peak I_{Ca} / C_m), was significantly smaller in RIM1/2 cDKO calyces as compared to control mice (Fig. 2F, $p < 0.001$).

Since RIM1 α expression was shown to reduce voltage-dependent inactivation of Ca^{2+} channels in BHK cells (Kiyonaka et al., 2007), we next tested whether the reduced Ca^{2+} current amplitude might result from an increased steady-state inactivation at the standardly employed holding potential of -70 mV. Conditioning pre-pulses of 2 s duration to more hyperpolarized membrane potentials (-90 mV, -110 mV; Fig. 2G, H) did not significantly increase the Ca^{2+} current during a subsequent step to 0 mV, arguing against significant steady-state inactivation at the holding potential. Therefore, the reduced Ca^{2+} current amplitude most likely reflects a reduced number of Ca^{2+} channels in the calyx of Held nerve terminals. With conditioning pre-pulses to more positive membrane potentials (-50 and -30 mV), we found a somewhat stronger steady-state inactivation in RIM1/2 cDKO calyces as compared to control (Fig. 2H; $p < 0.01$), consistent with previous work in cultured non-neuronal cells (Kiyonaka et al., 2007). Overall, however, our data failed to show a strong effect of RIM1/2 removal on the inactivation of presynaptic Ca^{2+} currents, at least for short depolarizing steps of up to 20 ms lengths (Fig. 2C).

In wild-type calyces of Held, about 80% of the presynaptic Ca^{2+} current is mediated by P/Q-type Ca^{2+} channels, and N- and R-type Ca^{2+} channels make up the rest (Wu et al., 1999; Iwasaki et al., 2000). To test whether the reduction of the presynaptic Ca^{2+} current is accompanied by a change in the contribution of Ca^{2+} channel subtypes, we blocked Ca^{2+} currents sequentially with the P/Q-type specific toxin ω -agatoxin-IVa (agatoxin; $0.2 \mu\text{M}$; Fig. 2I, green traces) followed by the N-type specific toxin ω -conotoxin-GVIA (conotoxin; $3 \mu\text{M}$) in the continued presence of agatoxin (Fig. 2I; blue traces). In RIM1/2 cDKO calyces, 80.6 ± 14 % of the Ca^{2+} current was blocked by agatoxin, similar to the value in control calyces (92 ± 7.1 %; $p = 0.14$; Fig. 2J). Another 14.7 ± 10.3 % of the initial Ca^{2+} current in RIM1/2 cDKO calyces was blocked by conotoxin, as compared to 8.2 ± 7.2 % in control calyces. Thus, removal of RIM1/2 does not significantly alter the relative contribution of P/Q- and N-type Ca^{2+} channels. Taken together, direct recordings from the nerve terminal reveal a strong reduction of presynaptic Ca^{2+} currents in RIM1/2 cDKO neurons, which is specific for the nerve terminal since Ca^{2+} currents in the soma/dendritic compartment of MNTB neurons were unchanged (Fig. S2). Thus, RIM proteins have a so far unrecognized role in enriching voltage-gated Ca^{2+} channels at the presynaptic nerve terminal (see also Kaeser et al., submitted).

RIMs ensure a large readily-releasable pool and influence release probability

We showed that conditional removal of RIM1/2 leads to a strong reduction of transmitter release (by ~ 80 %; Fig. 1), and that presynaptic Ca^{2+} currents are strongly reduced (~ 50 %; Fig. 2). Does the reduced transmitter release primarily reflect a reduced release probability caused by the much smaller presynaptic Ca^{2+} influx, or are there other factors, like a reduced readily-releasable pool of vesicles (Calakos et al., 2004), which contribute to the decreased transmitter release? To investigate changes in pool size and release probability, we next used brief high-frequency trains of afferent fiber stimulation to measure the size of the readily-releasable pool (Fig. 3; Schneggenburger et al., 1999). In control synapses, the

first EPSC was large (~ 8 nA in Fig. 3A), and subsequent EPSCs decreased in amplitude to a new steady-state value (Fig. 3A, B, right). In contrast, RIM1/2 cDKO synapses had much smaller EPSCs (~ 2 nA in Fig. 3A), and depression usually only occurred after the third or fourth stimulus (Fig. 3A, B, left; see also Fig. 3D for the average over all cells). To quantify the onset of depression, we made line fits to relative depression curves in the range of the first to the sixth stimulus (Fig. 3B, blue fit lines). This analysis gave slopes of -62 ± 26 % per 5 stimuli ($n = 8$) and -27 ± 33 % per 5 stimuli ($n = 9$) for control, and RIM1/2 cDKO synapses, respectively ($p < 0.05$; see also Fig. 3D, bottom, for line fits to the averaged data sets for each genotype). Thus, the onset of depression was significantly slowed in RIM1/2 cDKO synapses, which suggests a decreased release probability of any given readily-releasable vesicle.

We next analyzed the apparent size of the readily-releasable pool by using the method of cumulative EPSC amplitudes back-extrapolated to time zero (Schneppenburger et al., 1999; Fig. 3C). The back-extrapolated cumulative EPSC amplitude was 51.1 ± 16.2 nA in control mice (corresponding to ~ 1700 vesicles assuming an average mEPSC amplitude of 30 pA; $n = 8$ cells), but only 11.9 ± 6.9 nA in RIM1/2 cDKO mice (~ 400 vesicles; $n = 10$ cells). Thus, there was a clear pool size reduction in RIM1/2 cDKO synapses ($p < 0.001$; Fig. 3E). The average release probability, calculated by dividing the first EPSC amplitude by the pool size estimate (Iwasaki and Takahashi, 2001), was 0.27 ± 0.09 ($n = 8$) and 0.19 ± 0.05 ($n = 9$) in control and RIM1/2 cDKO synapses, respectively ($p = 0.04$; Fig. 3F). These experiments with high-frequency trains show that the release deficit is primarily caused by a decreased pool of readily-releasable vesicles (reduction by ~ 75 %; Fig. 3E). In addition, there was also a small but significant reduction of the release probability (by ~ 25 %), which might explain the observed slowing in the onset of synaptic depression.

Ca²⁺ uncaging reveals a smaller fast-releasable pool and a decreased Ca²⁺ sensitivity of release

We showed that in the absence of RIM1/2, the number of presynaptic Ca²⁺ channels was reduced ~ 50 % (Fig. 2), and the readily-releasable pool was strongly reduced, together with a small reduction of the release probability (Fig. 3). To study the reduced readily-releasable pool size more directly, we used Ca²⁺ uncaging to strongly stimulate release independent of Ca²⁺ channel opening. In addition, Ca²⁺ uncaging will allow us to address the possibility of a reduced intrinsic Ca²⁺ sensitivity of release in RIM1/2 cDKO synapses, which could underlie the reduced release probability.

In RIM1/2 cDKO synapses, Ca²⁺ uncaging stimuli evoked EPSCs with small amplitudes (~ 6 nA in the example of Fig. 4B, left), and flashes that elevated $[Ca^{2+}]_i$ above ~ 15 μ M did not evoke EPSCs with larger amplitudes in RIM1/2 cDKO synapses (Fig. 4B), showing directly the limited pool of readily-releasable vesicles in RIM1/2 cDKO synapses. The maximal EPSC amplitudes at $10 - 15$ μ M $[Ca^{2+}]_i$ were much smaller in RIM1/2 cDKO synapses (5.7 ± 4.9 nA, $n = 7$) than in control synapses (14.2 ± 7.8 nA, $n = 6$; $p < 0.01$), indicating a reduced pool size. To analyze the number of releasable vesicles and their release kinetics in more detail, we deconvolved the Ca²⁺ uncaging-evoked EPSCs to reveal rates of transmitter release (Fig. 4B, inset) and cumulative release rates (Fig. 4C). These were best fitted by the sum of at least two exponential functions (see Experimental Procedures), indicating a fast- and a slow release component in response to Ca²⁺ uncaging (Wölfel et al., 2007; Kochubey et al., 2009). Thus, the pool of readily-releasable vesicles can be kinetically subdivided into a fast- and a slowly releasable pool, FRP and SRP (Sakaba and Neher, 2001; Wölfel et al., 2007). To estimate the size of the FRP, we analyzed the number of vesicles released in the fast release component in response to $[Ca^{2+}]_i$ steps to $10 - 15$ μ M. The FRP was strongly reduced, from 1091 ± 396 vesicles in control synapses, to 271 ± 178 vesicles in RIM1/2 cDKO synapses ($n = 6$ and 7 respectively; Fig. 4D). In addition, the amplitude of

the slow release component was also reduced, from 833 ± 658 to 211 ± 205 vesicles in control and RIM1/2 cDKO synapses, respectively ($p = 0.036$).

We next plotted the absolute peak release rates as a function of the presynaptic $[Ca^{2+}]_i$ step amplitude (Fig. 4E). This plot showed that the peak release rates were significantly smaller at all $[Ca^{2+}]_i$ in RIM1/2 cDKO synapses as compared to control ($p < 0.001$; analysis of covariance, ANCOVA). However, the absolute peak release rates at any given $[Ca^{2+}]_i$ are a function of the intrinsic Ca^{2+} sensitivity of release, as well as of the absolute pool size. Therefore, to normalize for the reduced FRP size, we divided the absolute peak release rates by the FRP estimated in each cell pair. This revealed slightly reduced pool-normalized release rates in RIM1/2 cDKO synapses (Fig. 4F), but this difference did not reach statistical significance ($p = 0.13$; ANCOVA). In contrast, other kinetic parameters of release, like the minimal delay and the fast release time constant, showed a significant slowing at all $[Ca^{2+}]_i$ investigated ($p < 0.001$ and $p < 0.01$; see Fig. 4G, H), indicating that the intrinsic Ca^{2+} sensitivity of release was lower in the absence of RIM1/2.

To analyze the lowered intrinsic Ca^{2+} sensitivity quantitatively, the kinetic data, as well as the pool-normalized peak release rates, were globally fitted by a model of cooperative Ca^{2+} binding and vesicle fusion (Schneggenburger and Neher, 2000). The fits showed that a lowering of the on rate of Ca^{2+} binding (k_{on}) and a slight lowering of the off rate (k_{off}) led to a good description of the RIM1/2 cDKO data as compared to the control synapses (Fig. 4F, G, H; red and black fit lines, respectively; see Experimental Procedures for model parameters). The Ca^{2+} uncaging experiments therefore show that RIM1/2 proteins determine the size of the readily-releasable pool since both the FRP and SRP were reduced, and RIM1/2 increases the intracellular Ca^{2+} - sensitivity of release by a factor of ~ 1.5 to 2 - fold.

RIM proteins contribute to Ca^{2+} channel - vesicle coupling

We have shown that RIM proteins are necessary to enrich Ca^{2+} channels at the presynaptic nerve terminal (Fig. 2), and to maintain a high number of readily-releasable vesicles (Figs 3, 4). How well are the remaining readily-releasable vesicles coupled to the remaining Ca^{2+} channels? To address this question, we made paired pre- and postsynaptic recordings and performed a kinetic analysis of transmitter release in response to Ca^{2+} influx through voltage-gated Ca^{2+} channels (Fig. 5). Analyzing such data in the light of the intracellular Ca^{2+} sensitivities as determined by Ca^{2+} uncaging for each genotype (Fig. 4), should then allow us to examine the efficiency of the coupling between Ca^{2+} channels and readily-releasable vesicles (Wadel et al., 2007).

In most experiments, the presynaptic membrane potential was briefly stepped to +80 mV to open Ca^{2+} channels rapidly, and then returned to 0 mV to admit a pulse-like presynaptic Ca^{2+} influx (Fig. 5A, B, top; Sakaba and Neher, 2001). As expected, the resulting Ca^{2+} currents were smaller in RIM1/2 cDKO calyces (Fig. 5A, top), and the EPSCs in response to such pool-depleting Ca^{2+} currents were significantly smaller in RIM1/2 cDKO synapses (6.8 ± 2.4 nA; $n = 6$) as compared to control (25.9 ± 6.4 nA; $n = 5$; $p < 0.001$), indicative of the reduced pool size (see above). Interestingly, the 20 – 80% rise time of the EPSCs was prolonged in RIM1/2 cDKO synapses (3.4 ± 1.5 ms; $n = 6$) as compared to control synapses (1.24 ± 0.4 ms, $n = 5$; $p = 0.012$), which indicates an additional deficit in the kinetics of transmitter release.

To investigate the defects in release kinetics in more detail, we deconvolved the EPSCs to derive transmitter release rates (Fig. 5B, black traces), and traces of cumulative release (Fig. 5C, black trace below blue fit line). The peak release rates were strongly reduced in RIM1/2 cDKO synapses (Fig. 5D) and the width of the transmitter release at half-maximal

amplitudes was longer in RIM1/2 cDKO synapses (5.1 ± 1.8 ms, $n = 6$) than in control (2.3 ± 1.1 ms, $n = 5$; $p < 0.05$). The integrated release rate traces were fitted with a series of single- and double exponential function with or without line component, to determine the best fit function (see Experimental Procedures). In both genotypes, cumulative release was best fitted by functions which contained at least two exponential components (Fig. 5C, blue fit lines), indicating a fast- and a slow release component (Sakaba and Neher, 2001; Wadel et al., 2007; Wölfel et al., 2007). In RIM1/2 cDKO synapses, the fast release time constant was significantly slower (5.2 ± 1.7 ms, $n = 6$) than in control synapses (1.8 ± 0.8 ms, $n = 5$; Fig. 5E; $p = 0.002$), but it was significantly faster than the *slow* release time constant in control synapses, which was 23 ± 3.7 ms ($n = 5$; Fig. 5F; $p < 0.001$). Similarly, when cumulative release traces were arbitrarily fitted with monoexponential functions, the resulting time constant in RIM1/2 cDKO synapses (9.3 ± 1.1 ms; $n = 6$) was still significantly faster than the slow release time constant in wild-type cells ($p < 0.001$). Both of these comparisons show that the FRP is not simply missing completely, but rather, that release from the remaining FRP is slowed in the RIM1/2 cDKO synapses. Figure 5 (E, F) shows further parameters extracted from the kinetic analysis of transmitter release for each genotype. Overall, the analysis shows a strongly reduced number of readily-releasable vesicles in both the FRP and the SRP, as well as a significant, ~ 2.5 -fold slowing of the fast release component.

The kinetics of transmitter release in response to Ca^{2+} influx depends on the intrinsic speed of release, as well as on the 'local' $[\text{Ca}^{2+}]_i$ that builds up close to the readily-releasable vesicles, which, in turn, is a function of the distance between Ca^{2+} channels and vesicles (Neher, 1998; Wadel et al., 2007). The Ca^{2+} uncaging experiments showed that the intrinsic Ca^{2+} sensitivity is reduced in the absence of RIM1/2 (Fig. 4). To ask whether the spatial coupling between Ca^{2+} channels and vesicles was impaired as well, we back-calculated the 'local' $[\text{Ca}^{2+}]_i$ that was necessary to reproduce the kinetics of the fast release component in response to depolarizations (Fig. 5B, C; grey traces; Schneggenburger and Neher, 2000). This was done by using the specific sets of kinetic parameters which describe the intracellular Ca^{2+} sensitivities of transmitter release of RIM1/2 cDKO - and control synapses (Fig. 4). In the examples of Fig. 5C, a step-like local $[\text{Ca}^{2+}]_i$ signal of $7.7 \mu\text{M}$ predicted the time-course of the fast release component in the RIM1/2 cDKO synapse, whereas a $[\text{Ca}^{2+}]_i$ signal of $9.4 \mu\text{M}$ was necessary in the case of the control synapse. On average, the back-calculated local $[\text{Ca}^{2+}]_i$ signal was $12.0 \pm 2.5 \mu\text{M}$ ($n = 5$) and $9.0 \pm 1.2 \mu\text{M}$ ($n = 6$) in control - and RIM1/2 cDKO synapses, respectively (Fig. 5G; $p < 0.05$). Thus, the local $[\text{Ca}^{2+}]_i$ signal experienced by average readily-releasable vesicles during a Ca^{2+} current at 0 mV is significantly smaller in RIM1/2 cDKO synapses. This suggests that there are either fewer 'local' Ca^{2+} channels around each given readily-releasable vesicle, and/or that the average distance between Ca^{2+} channels and vesicles is increased in the absence of RIM1/2.

In further experiments designed to analyze a decreased coupling between Ca^{2+} channels and vesicles, we measured the suppression of EPSCs by the slow Ca^{2+} buffer, EGTA-AM (Fig. S3). These experiments showed a trend towards a faster block by EGTA-AM in RIM1/2 cDKO synapses, as would be expected for a longer Ca^{2+} channel - vesicle distance (Borst and Sakmann, 1996; Fedchyshyn and Wang, 2005); however, the difference did not reach statistical significance ($p = 0.073$).

RIMs dock vesicles to the active zone

We showed that RIM1/2 deletion led to a strong reduction of the readily-releasable pool (Figs 3–5). Does this reduction of the functional pool size reflect a deficit in "priming" docked vesicles to fusion competence as suggested before (Koushika et al., 2001; Calakos et al., 2004); or else, might RIM proteins have an additional role in vesicle docking? To

distinguish between these possibilities, we investigated the synaptic ultrastructure of RIM1/2 cDKO calyces and control calyces using serial section transmission electron microscopy (EM) (Fig. 6). Large calyx of Held nerve terminals in the MNTB area of both genotypes had overall normal appearance (not shown). In high-resolution images of active zones, there was a conspicuous reduction in the number of vesicles at active zones, and fewer docked vesicles were apparent (Fig. 6A), suggesting that RIM1/2 is involved in vesicle docking.

To quantify the spatial distribution of vesicles, we reconstructed entire active zones, taking into account all detected vesicles within a distance of 300 nm to the active zone membrane (Fig. 6B). From the reconstructions, histograms of the shortest membrane-to-membrane distance between each vesicle and the active zone were computed (Fig. 6C; $n = 18$ and 17 active zones for RIM1/2 cDKO and control tissue, sampled over $n = 4$ calyces each). For the control data, there was a clear peak for the membrane - nearest bin (10 nm or less; Fig. 5C, arrow), which most likely represents the pool of docked vesicles (Verhage and Sorensen, 2008). Importantly, in RIM1/2 cDKO synapses, the vesicle number in this membrane-near bin was strongly reduced (Fig. 6C; arrow). Fig. 6D shows the relative vesicle number (RIM1/2 cDKO / control * 100 for each bin), which illustrates a quite selective decrease in the membrane-near bin, although there was also a modest decrease in the number of vesicles located further away in the cytoplasm (~ 20%; Fig. 5D). Defining "docked" vesicles as those that are located within 10 nm of the active zone membrane, we found 7.0 ± 4.6 docked vesicles in control synapses ($n = 17$ active zones), but only 1.5 ± 1.8 in RIM1/2 cDKO synapses ($n = 18$; Fig. 6E; $p < 0.001$). This shows a drastic reduction of the number of vesicles docked at the active zone membrane in RIM1/2 cDKO synapses.

In *c.elegans* synapses, RIM1 enables the lateral localization of docked vesicles close to a central membrane specialization of the active zone (Gracheva et al., 2008). In analogy, it is possible that in mammalian synapses, the loss of RIM proteins could lead to a lateral mis-localization of docked vesicles into areas adjacent to the active zone ("outliers"). To address this possibility, we made flat surface renderings of each three-dimensionally reconstructed active zone and its adjacent plasma membrane (Fig. 6F), and then analyzed the density of "outlier" docked vesicles, which were defined as docked vesicles localized up to 100 nm outside of active zones (Fig. 6F, see green symbols). As can be seen in the example images in Fig. 6F, active zone size varied greatly between individual contact sites (Schikorski and Stevens, 1997; Taschenberger et al., 2002), but the average active zone size was unchanged between the genotypes (Fig. 6G, H). Overall, we only found $n = 8$ and $n = 9$ outlier vesicles in the set of $n = 17$ and 18 active zones analyzed here. Normalized to the corresponding membrane area, the density of outliers was similarly low for both genotypes (~ 3 – 4 vesicles / μm^2 ; see TableS1); note that this value is less than 5% of the density of docked vesicles within the active zones of wild-type synapses (Fig. 6I). Thus, removal of RIM proteins specifically reduces the density of docked vesicles within the active zone (Fig. 5I, $p < 0.001$), but does not affect the number of vesicles docked adjacent to the active zone.

Discussion

We have established a Cre-lox based conditional KO approach at a presynaptically accessible CNS synapse, the calyx of Held. This has allowed us to use presynaptic recordings and Ca^{2+} uncaging, as well as EM analyses of synapses which have developed *in vivo*, to directly study the presynaptic functions of RIM proteins. We have found three main roles of RIM proteins: First, the presynaptic Ca^{2+} current density was strongly reduced about two-fold in RIM1/2 cDKO nerve terminals. This, together with the accompanying paper by Kaeser et al. (submitted to *Cell*), establishes an important role for RIM proteins in localizing Ca^{2+} channels to the active zone. Second, we find a reduced pool of readily-releasable vesicles in agreement with previous studies (Calakos et al., 2004), and a

decreased number of membrane-near vesicles at the active zone, revealing a vesicle docking function of RIM proteins. Third, RIM proteins speed the rate of transmitter release by increasing the intrinsic Ca^{2+} -sensitivity of release, as well as by contributing to the tight co-localization of readily-releasable vesicles with Ca^{2+} channels. Taken together, our study shows that RIM proteins coordinately regulate Ca^{2+} channel targeting, vesicle docking and priming, and Ca^{2+} channel - vesicle co-localization at the presynaptic active zone.

Conditional knock out approach at the calyx of Held

For the generation of calyx-specific conditional knock-out mice, we have made use of recently generated floxed mouse lines for RIM1 $\alpha\beta$ (Kaeser et al., 2008) and RIM2 $\alpha\beta\gamma$ (Kaeser et al., submitted), and of a previously available Cre knock-in mouse line in the Krox20 locus (Voiculescu et al., 2000). The presynaptic neuron pool that generates the large calyx of Held nerve terminals onto MNTB neurons is located in the contralateral VCN, and is largely represented by globular bushy cells (Cant and Benson, 2003). Krox20 is a transcription factor that is highly specifically active in rhombomeres 3 and 5 of the developing hindbrain (Voiculescu et al., 2000), which give rise to a majority of neurons in the VCN (Farago et al., 2006; Maricich et al., 2009). We found homogeneous phenotypes amongst the recorded calyx of Held synapses, which indicates, together with morphological analysis (Fig. 1B; L. Xiao, N. Michalski & R.S., unpublished observations; Renier et al., 2010) that the entire population of calyx of Held - generating neurons stems from Krox20Cre positive neurons. Thus, the Krox20Cre mouse line allows to conditionally remove floxed alleles at the calyx of Held synapse, which will make it a useful tool to advance our understanding also of other proteins of the presynaptic vesicle cycle.

RIM proteins localize Ca^{2+} channels to the active zone

Using direct presynaptic recordings at the nerve terminal, we demonstrated that RIM proteins are essential for localizing Ca^{2+} channels to the active zone, as shown by the clear decrease in the presynaptic Ca^{2+} current density in RIM1/2 cDKO calyces. These direct recordings at the nerve terminal show that RIMs determine presynaptic Ca^{2+} channel density without changing major biophysical parameters of Ca^{2+} channel gating, although we cannot exclude that RIMs influence Ca^{2+} channel inactivation with prolonged pulses (> 50 ms, Fig. 2; Kiyonaka et al., 2007); this, however, will be relevant only for prolonged presynaptic AP trains. Analyzing RIM-dependent presynaptic Ca^{2+} channel targeting has been limited because previously no KO mice deleting all RIM1/2 isoforms were available (Schoch et al., 2002; Calakos et al., 2004), and because previously investigated synapses, including the *C. elegans* neuromuscular synapse (Koushika et al., 2001), did not allow for measurements of presynaptic Ca^{2+} currents. Using cultured RIM1/2 cDKO neurons, Kaeser et al. (*submitted to Cell*) have observed an about two-fold reduction in Ca^{2+} transients in presynaptic boutons during an AP, and observed an equal reduction in the staining intensity with anti- $\alpha 1A$ Ca^{2+} channel subunit antibodies. This, together with our finding that presynaptic APs are unchanged (Fig. 2), is evidence for a reduced Ca^{2+} channel density also at small bouton-like synapses. We conclude that the role of RIM1/2 proteins in enriching Ca^{2+} channels at the nerve terminal is a widespread mechanism found at many CNS synapses including the calyx of Held, and hippocampal excitatory and inhibitory synapses (Kaeser et al., *submitted*).

What might be the molecular mechanism by which RIM proteins hold Ca^{2+} channels at the active zone? In a parallel study, Kaeser et al. (*submitted*) showed that the RIM1 and RIM2 PDZ domains directly bind to the C-terminal sequences of the P/Q- and N-type Ca^{2+} channel α -subunits, and that the PDZ domain was required to rescue the decreased Ca^{2+} transients and the abnormal Ca^{2+} channel localization. In addition, the proline-rich domain of RIM1/2 was also necessary for the rescue, suggesting that a tripartite interaction between RIM1/2, RIM-BPs (which bind to the proline-rich domain of RIMs; Hibino et al., 2002) and

the Ca²⁺ channel α subunits is critical for the Ca²⁺ channel targeting function of RIM1/2 (Kaeser et al., *submitted*). This, together with the present work identifies RIM1/2 as a presynaptic scaffolding proteins with a clear role in maintaining a high Ca²⁺ channel density at the presynaptic active zone. Previous work has suggested a role for Bruchpilot, a drosophila gene related to ELKS/CAST proteins, in maintaining presynaptic Ca²⁺ channel density and structural entirety at drosophila presynaptic active zones (Kittel et al., 2006).

Conditional removal of RIM1/2 did not significantly change the relative contribution of P/Q-type - and N-type channels to the total presynaptic Ca²⁺ current, despite a strongly reduced total Ca²⁺ current. This finding is different to the situation in P/Q-type (α 1A-subunit) KO mice (Jun et al., 1999), in which a strong compensatory upregulation of presynaptic N-type channels was observed at the calyx of Held (Inchauspe et al., 2004; Ishikawa et al., 2005). Thus, in the absence of RIM1/2, N-type Ca²⁺ channels are not capable to compensate for the missing P/Q-type channels and therefore, the absence of RIM1/2 likely affects both Ca²⁺ channel α subunits equally. This agrees with the finding by Kaeser et al. (*submitted*) who showed that RIM1/2 binds to both P/Q- and N-type channel α -subunits.

RIMs' function in vesicle docking and formation of the readily-releasable pool

The calyx synapse has been an ideal preparation to functionally define a fast and a slow subpool of the readily-releasable pool (Sakaba and Neher, 2001; Wölfel et al., 2007; Wadel et al., 2007; see Neher, 2006 for a review). Here, we find that conditional removal of all major RIM isoforms leads to a strong, ~ 70% decrease of the readily-releasable pool size as defined by various types of pool-depleting Ca²⁺ stimuli (Figs 3–5). Importantly, we found a very similar decrease of the number of docked vesicles at the active zone (by ~ 70%; Fig. 6), demonstrating a genetic manipulation that leads to a parallel decrease in the number of docked vesicles, and of the readily-releasable pool size determined functionally. Thus, at the calyx of Held, the amount of vesicle docking seems to determine the size of the readily releasable pool. This conclusion is further supported by the reasonable quantitative agreement between the number of docked vesicles on the one hand (~ 7 docked vesicle per active zone * 500 \approx 3500; assuming that a calyx has ~ 500 active zones; Sätzler et al., 2002; Taschenberger et al., 2002), and the sum of FRP and SRP vesicles on the other hand (~ 3000 – 3500; see Fig. 5). This indicates that most docked vesicles belong to the readily-releasable pool at the wild-type calyx of Held. Genetic removal of all RIM1/2 isoforms strongly reduced docking, and thereby determined the size of the readily-releasable pool. This conclusion does not rule out the possibility that an additional priming step is necessary to make docked vesicles fusion-competent (see Südhof, 2004 for review), and that RIMs might have an additional role in vesicle priming (Koushika et al., 2001; Calakos et al., 2004).

Further work is needed to unravel the molecular mechanisms by which RIM determines vesicle docking, and how vesicle docking and priming are related to each other. The long isoforms of RIMs interact via their N-termini with Munc13, and with the small GTPase Rab3 (Wang et al., 1997; Dulubova et al., 2005) and related Rab's including Rab8A, -10, and -26 (Fukuda, 2003). It is thought that the interaction of RIMs with Munc13 is important for priming docked vesicles to fusion competence (Betz et al., 2001), since Munc13 was described as a priming factor with no role in vesicle docking (Augustin et al., 1999). However, recent studies on Munc13 suggested also a role in docking (Siksou et al., 2009), somewhat blurring the distinction between vesicle docking and priming. Single Rab3A KO mice exhibit a deficit in the activity-dependent recruitment of docked vesicles in synaptosomes (Leenders et al., 2001) and show a vesicle docking phenotype at the neuromuscular junction (Coleman et al., 2007), but surprisingly, quadruple Rab3A/B/C/D KO mice do not exhibit a docking phenotype in cultured hippocampal neurons (Schlüter et al., 2004). Taken together, the interaction of the long RIM isoforms with Rab3 and related

Rabs could explain the docking function of RIM proteins, and it is possible that in RIM1 α KO mice (Schoch et al., 2002) the docking deficit was compensated by the continued presence of RIM1 β , 2 α , and 2 β . Thus, our experiments in the context of previous data show that RIM proteins have an important role in vesicle docking.

RIMs influence release probability and the intrinsic Ca²⁺-dependent speed of release

A third role of RIM proteins regards the release probability of any given readily-releasable vesicle. Kinetic analysis showed a clear slowing of the release of the remaining FRP vesicles in RIM1/2 cDKO synapses (Fig. 5). This was mediated, in part, by a reduction of the intracellular Ca²⁺ sensitivity of release demonstrated in Ca²⁺ uncaging experiments (Fig. 4), mediated by a so far unknown molecular mechanism of RIM. In addition, there was a defect in the coupling between Ca²⁺ channels and vesicles for FRP vesicles, visible as a decreased 'local' [Ca²⁺]_i signal that we back-calculated during stimulation of release with presynaptic depolarizations (Fig. 5). Thus, RIM proteins contribute to a tight Ca²⁺ channel - vesicle colocalization, a function which likely reflects the interaction of RIMs with Ca²⁺ channels on the one hand (see above; Kaeser et al., *submitted*), and with vesicle proteins like Rab3 on the other hand.

Taken together, establishing a conditional KO approach at a presynaptically accessible CNS synapse has allowed us to dissect multiple intertwined roles of the presynaptic scaffolding protein RIM1/2. Overall, the interaction of RIM proteins with a large number of presynaptic proteins (Schoch et al., 2002) allow RIMs to influence several important functions vital for fast transmitter release: first, the targeting of Ca²⁺ channels to the active zone, likely mediated by interactions of the central RIM1/2 PDZ domain with Ca²⁺ channel α -subunits (Kaeser et al., *submitted*); second, vesicle docking and the formation of a standing readily-releasable pool important for maintaining fast release during repeated stimuli (Sorensen, 2004); and third, intrinsic speeding of release and a tighter coupling between vesicles and Ca²⁺ channels. Thus, RIM proteins coordinate multiple functions late in the vesicle cycle which all guarantee a fast speed of Ca²⁺ evoked release at CNS synapses.

Experimental Procedures

Conditional RIM1/2 KO mice specific for the auditory brainstem

We identified the Krox20Cre mouse line (Voiculescu et al., 2000); gift of Dr. Patrick Charnay, Paris, France) as a suitable Cre mouse line which drives Cre expression in calyx of Held - generating neurons of the VCN (Fig. 1A, and Fig. S1). We crossed heterozygous Krox20+/Cre mice with a mouse line which carried a floxed RIM1 allele (Kaeser et al., 2008), as well as a floxed RIM2 allele (Kaeser et al., *submitted*) (see also Supplementary Experimental Procedures). The offspring of the final breeding pairs gave rise to an expected 50 % Cre-positive, RIM1lox/ Δ , RIM2lox/ Δ mice. Due to germline recombination in the Krox20Cre line (Voiculescu et al., 2000), one of each floxed RIM allele was deleted in these mice as confirmed by PCR-based genotyping. Synapses recorded in these mice are referred to as RIM1/2 cDKO synapses (for conditional double KO). Since Cre-expression turns on at ~ E11 in Krox20+/Cre mice (Voiculescu et al., 2000), the floxed RIM1/2 alleles should be deleted even before synapses initially form at ~ E17 in brainstem. As control mice, we used Cre-negative littermate mice with otherwise the same genetic background; thus, the control mice were heterozygous with respect to the RIM alleles. Cre-positive, RIM1lox/ Δ , RIM2lox/ Δ mice were viable and fertile, and were used for further interbreeding. For the analysis of neuron populations in which Cre-recombinase was active, we crossed Krox20+/Cre mice with tdRFP reporter mice (Luche et al., 2007), and performed anti-RFP and anti-Syt2 immunohistochemistry (see Supplementary Experimental Procedures) to reveal Cre-positive neurons and nerve terminals (Fig. 1A, B; Fig. S1).

Slice preparation and electrophysiology

Transverse brainstem slices were prepared from postnatal (P) 9 – 11 days mice according to standard methods, using a LEICA VT1000S slicer. Paired pre- and postsynaptic whole-cell recordings at the calyx of Held synapse were made with an EPC10/double patch-clamp amplifier (HEKA), under visualization in an upright microscope (Zeiss Axioskop 2 FS) equipped with gradient contrast infrared visualization (Luigs & Neumann) and a 60× objective. Details on the electrophysiological methods, and on the composition of the patch pipette - and extracellular solutions are provided in Supplementary Experimental Procedures.

EPSC deconvolution and data analysis

Deconvolution of EPSCs to calculate the rates of transmitter release was done similarly as first described by (Neher and Sakaba, 2001), using routines written in IgorPro. The deconvolution analysis assumes that mEPSC with a double-exponential decay (Schneggenburger and Neher, 2000) add linearly to give rise to an evoked EPSC. The calculated release rates were corrected for a contribution of a spillover glutamate current as described (Neher and Sakaba, 2001). Cumulative release traces were obtained by simple integration of the transmitter release traces, without further correction for an assumed recovery process. Cumulative release traces were fitted with the following functions: single-exponential, exponential plus line, double-exponential, double-exponential plus line, and triple-exponential (Wölfel et al., 2007), and the best-fit function was selected based on the Bayesian information criterion (BIC; Kochubey et al., 2009). Data are reported as average \pm S.D. values, and statistical significance was evaluated with Student's t-test, and accepted at $p < 0.05$. For the comparison of release rates, release delays and fast release time constants between two data sets at various $[Ca^{2+}]_i$ (Fig. 4E–H), the data sets were double-logarithmized, and then assessed for statistical significance by analysis of covariance (ANCOVA). The Ca^{2+} uncaging data was fitted by a five-site model of Ca^{2+} binding and vesicle fusion (Schneggenburger and Neher, 2000). The following parameters were used for control / RIM1/2 cDKO synapses respectively: k_{on} , $1.65 * 10^8 / 1.05 * 10^8 [M^{-1}s^{-1}]$; k_{off} , $7000 / 5000 [s^{-1}]$; pool size, $315 / 1390$ vesicles. The remaining parameters were the same for both data sets (cooperativity factor b , 0.35; final fusion rate γ , $7000 s^{-1}$).

Presynaptic Ca^{2+} uncaging

Ca^{2+} uncaging was done with a DP-10 flash-lamp (Rapp Optoelektronik) according to standard procedures described before (Schneggenburger and Neher, 2000; Wölfel et al., 2007); details are given in Supplementary Experimental Procedures.

Electron microscopy

Transmission EM was performed in the MNTB area of a RIM1/2 cDKO mouse and its control cre-negative littermate (both at P11), using standard fixation and resin embedding procedures (see Supplementary Experimental Procedures). Serial images were taken with a Philips CM10 TEM operated at 80 kV at a magnification of 16000 times, using 10 – 20 adjacent sections. Only active zones that were completely contained in the series were analyzed. The image series were aligned and active zones, including vesicles and surrounding plasma membrane, were reconstructed in 3D with the Fiji software (http://pacific.mpi-cbg.de/wiki/index.php/Main_Page). The shortest distance from the vesicle membrane to the active zone membrane was then calculated in the 3D model, and all vesicles at distances of less than 300 nm were taken into account. Flat rendering of the active zone surface was done by a MatLab function.

Supplementary Material

Refer to Web version on PubMed Central for supplementary material.

Acknowledgments

We thank Heather Murray for expert technical assistance; Dr. Graham Knott (Center for Interdisciplinary Electron Microscopy; EPFL) for help and advice with EM; Dr. Daniel Keller for help with flat surface rendering of active zone profiles; Dr. Patrick Charnay and Dr. Hans Jörg Fehling for the gift of mouse lines, and Dr. Olexiy Kochubey, Dr. Erwin Neher and Dr. David Perkel for comments on the manuscript. This research was supported by grants from the Swiss National Science Foundation (SNF; 31003A_122496) and the Synapsis foundation (both to R.S.).

References

- Augustin I, Rosenmund C, Südhof TC, Brose N. Munc13-1 is essential for fusion competence of glutamatergic synaptic vesicles. *Nature*. 1999; 400:457–461. [PubMed: 10440375]
- Betz A, Thakur P, Junge HJ, Ashery U, Rhee JS, Scheuss V, Rosenmund C, Rettig J, Brose N. Functional interaction of the active zone proteins Munc13-1 and RIM1 in synaptic vesicle priming. *Neuron*. 2001; 30:183–196. [PubMed: 11343654]
- Borst JG, Sakmann B. Calcium influx and transmitter release in a fast CNS synapse. *Nature*. 1996; 383:431–434. [PubMed: 8837774]
- Bucurenciu I, Kulik A, Schwaller B, Frotscher M, Jonas P. Nanodomain coupling between Ca²⁺ channels and Ca²⁺ sensors promotes fast and efficient transmitter release at a cortical GABAergic synapse. *Neuron*. 2008; 57:536–545. [PubMed: 18304483]
- Calakos N, Schoch S, Südhof TC, Malenka RC. Multiple roles for the active zone protein RIM1 α in late stages of neurotransmitter release. *Neuron*. 2004; 42:889–896. [PubMed: 15207234]
- Cant NB, Benson CG. Parallel auditory pathways: projection patterns of the different neuronal populations in the dorsal and ventral cochlear nuclei. *Brain Res Bull*. 2003; 60:457–474. [PubMed: 12787867]
- Castillo PE, Schoch S, Schmitz F, Südhof TC, Malenka RC. RIM1 α is required for presynaptic long-term potentiation. *Nature*. 2002; 415:327–330. [PubMed: 11797010]
- Chen YA, Scheller RH. SNARE-mediated membrane fusion. *Nat Rev Mol Cell Biology*. 2001; 2:98–106.
- Coleman WL, Bill CA, Bykhovskaia M. Rab3a deletion reduces vesicle docking and transmitter release at the mouse diaphragm synapse. *Neuroscience*. 2007; 148:1–6. [PubMed: 17640821]
- Coppola T, Magnin-Luthi S, Perret-Menoud V, Gattesco S, Schiavo G, Regazzi R. Direct interaction of the Rab3 effector RIM with Ca²⁺ channels, SNAP-25, and synaptotagmin. *J Biol Chem*. 2001; 276:32756–32762. [PubMed: 11438518]
- Dulubova I, Lou X, Lu J, Huryeva I, Alam A, Schneggenburger R, Südhof TC, Rizo J. A Munc13/RIM/Rab3 tripartite complex: from priming to plasticity? *EMBO J*. 2005; 24:2839–2850. [PubMed: 16052212]
- Farago AF, Awatramani RB, Dymecki SM. Assembly of the brainstem cochlear nuclear complex is revealed by intersectional and subtractive genetic fate maps. *Neuron*. 2006; 50:205–218. [PubMed: 16630833]
- Fedchyshyn MJ, Wang L-Y. Developmental transformation of the release modality at the calyx of Held synapse. *J Neuroscience*. 2005; 25:4131–4140.
- Fukuda M. Distinct Rab binding specificity of Rim1, Rim2, rabphilin, and Noc2. Identification of a critical determinant of Rab3A/Rab27 recognition by Rim2. *J Biol Chem*. 2003; 278:15373–15380. [PubMed: 12578829]
- Gracheva EO, Hadwiger G, Nonet ML, Richmond JE. Direct interactions between *C. elegans* RAB-3 and Rim provide a mechanism to target vesicles to the presynaptic density. *Neuroscience Letters*. 2008; 444:137–142. [PubMed: 18721860]
- Hibino H, Pironkova R, Onwumere O, Vologodskaya M, Hudspeth AJ, Lesage F. RIM binding proteins (RBPs) couple Rab3-interacting molecules (RIMs) to voltage-gated Ca²⁺ channels. *Neuron*. 2002; 34:411–423. [PubMed: 11988172]

- Inchauspe CG, Martini FJ, Forsythe ID, Uchitel OD. Functional compensation of P/Q by N-type channels blocks short-term plasticity at the calyx of Held presynaptic terminal. *J Neuroscience*. 2004; 24:10379–10383.
- Ishikawa T, Kaneko M, Shin H-S, Takahashi T. Presynaptic N-type and P/Q-type Ca^{2+} -channels mediating synaptic transmission at the calyx of Held of mice. *J Physiology*. 2005; 568:199–209.
- Iwasaki S, Momiyama A, Uchitel OD, Takahashi T. Developmental changes in calcium channel types mediating central synaptic transmission. *J Neurosci*. 2000; 20:59–65. [PubMed: 10627581]
- Iwasaki S, Takahashi T. Developmental regulation of transmitter release at the calyx of Held in rat auditory brainstem. *J Physiology*. 2001; 534:861–871.
- Jahn R, Lang T, Südhof TC. Membrane fusion. *Cell*. 2003; 112:519–533. [PubMed: 12600315]
- Jun K, Piedras-Renteria ES, Smith SM, Wheeler DB, Lee SB, Lee TG, Chin H, Adams ME, Scheller RH, Tsien RW, Shin HS. Ablation of P/Q-type Ca^{2+} channel currents, altered synaptic transmission, and progressive ataxia in mice lacking the α_{1A} -subunit. *Proc Natl Acad Sci U S A*. 1999; 96:15245–15250. [PubMed: 10611370]
- Kaesler PS, Kwon HB, Chiu CQ, Deng L, Castillo PE, Südhof TC. RIM1 α and RIM1 β are synthesized from distinct promoters of the RIM1 gene to mediate differential but overlapping synaptic functions. *J Neuroscience*. 2008; 28:13435–13447.
- Kittel RJ, Wichmann C, Rasse TM, Fouquet W, Schmidt M, Schmid A, Wagh DA, Pawlu C, Kellner RR, Willig KI, et al. Bruchpilot promotes active zone assembly, Ca^{2+} channel clustering, and vesicle release. *Science*. 2006; 312:1051–1054. [PubMed: 16614170]
- Kiyonaka S, Wakamori M, Miki T, Uriu Y, Nonaka M, Bito H, Beedle AM, Mori E, Hara Y, De Waard M, et al. RIM1 confers sustained activity and neurotransmitter vesicle anchoring to presynaptic Ca^{2+} channels. *Nat Neurosci*. 2007; 10:1–11. [PubMed: 17189939]
- Kochubey O, Han Y, Schneggenburger R. Developmental regulation of the intracellular Ca^{2+} sensitivity of vesicle fusion and Ca^{2+} -secretion coupling at the rat calyx of Held. *J Physiol*. 2009; 587:3009–3023. [PubMed: 19403608]
- Koushika SP, Richmond JE, Hadwiger G, Weimer RM, Jorgensen EM, Nonet ML. A post-docking role for active zone protein Rim. *Nat Neurosci*. 2001; 4:997–1005. [PubMed: 11559854]
- Leenders AGM, Lopes da Silva FH, Ghijsen WEJM, Verhage M. Rab3A is involved in transport of synaptic vesicles to the active zone in mouse brain nerve terminals. *Mol Biol Cell*. 2001; 12:3095–3102. [PubMed: 11598194]
- Llinás R, Sugimori M, Silver RB. The concept of calcium concentration microdomains in synaptic transmission. *Neuropharmacology*. 1995; 34:1443–1451. [PubMed: 8606792]
- Luche H, Weber O, Nageswara Rao T, Blum C, Fehling HJ. Faithful activation of an extra-bright red fluorescent protein in "knock-in" Cre-reporter mice ideally suited for lineage tracing studies. *Eur J Immunol*. 2007; 37:43–53. [PubMed: 17171761]
- Maricich SM, Xia A, Mathes EL, Wang VY, Oghalai JS, Fritzsche B, Zoghbi HY. Atoh1-lineal neurons are required for hearing and for the survival of neurons in the spiral ganglion and brainstem accessory auditory nuclei. *J Neurosci*. 2009; 29:11123–11133. [PubMed: 19741118]
- Neher E. Vesicle pools and Ca^{2+} microdomains: New tools for understanding their roles in neurotransmitter release. *Neuron*. 1998; 20:389–399. [PubMed: 9539117]
- Neher E. A comparison between exocytotic control mechanisms in adrenal chromaffin cells and a glutamatergic synapse. *Pflügers Arch - Eur J Physiol*. 2006; 453:261–268.
- Neher E, Sakaba T. Combining deconvolution and noise analysis for the estimation of transmitter release rates at the calyx of Held. *J Neuroscience*. 2001; 21:444–461.
- Renier N, Schonewille M, Giraudet F, Badura A, Tessier-Lavigne M, Avan P, De Zeeuw CI, Chedotal A. Genetic dissection of the function of hindbrain axonal commissures. *PLoS Biol*. 2010; 8:e1000325. [PubMed: 20231872]
- Sabatini BL, Regehr WG. Timing of neurotransmission at fast synapses in the mammalian brain. *Nature*. 1996; 384:170–172. [PubMed: 8906792]
- Sakaba T, Neher E. Calmodulin mediates rapid recruitment of fast-releasing synaptic vesicles at a calyx-type synapse. *Neuron*. 2001; 32:1119–1131. [PubMed: 11754842]

- Sätzler K, Söhl LF, Bollmann JH, Borst JGG, Frotscher M, Sakmann B, Lübke JH. Three-dimensional reconstruction of a calyx of Held and its postsynaptic principal neuron in the medial nucleus of the trapezoid body. *J Neuroscience*. 2002; 22:10567–10579.
- Schikorski T, Stevens CF. Quantitative ultrastructural analysis of hippocampal excitatory synapses. *J Neurosci*. 1997; 17:5858–5867. [PubMed: 9221783]
- Schlüter OM, Schmitz F, Jahn R, Rosenmund C, Südhof TC. A complete genetic analysis of neuronal Rab3 function. *J Neuroscience*. 2004; 24:6629–6637.
- Schneggenburger R, Forsythe ID. The calyx of Held. *Cell and Tissue Res*. 2006; 326:311–337. [PubMed: 16896951]
- Schneggenburger R, Meyer AC, Neher E. Released fraction and total size of a pool of immediately available transmitter quanta at a calyx synapse. *Neuron*. 1999; 23:399–409. [PubMed: 10399944]
- Schneggenburger R, Neher E. Intracellular calcium dependence of transmitter release rates at a fast central synapse. *Nature*. 2000; 406:889–893. [PubMed: 10972290]
- Schoch S, Castillo PE, Jo T, Mukherjee K, Geppert M, Wang Y, Schmitz F, Malenka RC, Südhof TC. RIM1 α forms a protein scaffold for regulating neurotransmitter release at the active zone. *Nature*. 2002; 415:321–326. [PubMed: 11797009]
- Schoch S, Gundelfinger ED. Molecular organization of the presynaptic active zone. *Cell Tissue Res*. 2006; 326:379–391. [PubMed: 16865347]
- Schoch S, Mittelstaedt T, Kaeser PS, Padgett D, Feldmann N, Chevaleyre V, Castillo PE, Hammer RE, Han W, Schmitz F, et al. Redundant functions of RIM1 α and RIM2 α in Ca²⁺-triggered neurotransmitter release. *EMBO J*. 2006; 25:5852–5863. [PubMed: 17124501]
- Siksou L, Varoqueaux F, Pascual O, Triller A, Brose N, Marty S. A common molecular basis for membrane docking and functional priming of synaptic vesicles. *Eur J Neurosci*. 2009; 30:49–56. [PubMed: 19558619]
- Sorensen JB. Formation, stabilization and fusion of the readily releasable pool of secretory vesicles. *Eur J Physiol*. 2004; 448:347–362.
- Südhof TC. The synaptic vesicle cycle. *Annu Rev Neurosci*. 2004; 27:509–547. [PubMed: 15217342]
- Taschenberger H, Leao RM, Rowland KC, Spirou GA, Gersdorff H. Optimizing synaptic architecture and efficiency for high-frequency transmission. *Neuron*. 2002; 36:1127–1143. [PubMed: 12495627]
- Verhage M, Sorensen JB. Vesicle docking in regulated exocytosis. *Traffic*. 2008; 9:1414–1424. [PubMed: 18445120]
- Voiculescu O, Charnay P, Schneider-Maunoury S. Expression pattern of a Krox-20/Cre knock-in allele in the developing hindbrain, bones, and peripheral nervous system. *Genesis*. 2000; 26:123–126. [PubMed: 10686605]
- Wadel C, Neher E, Sakaba T. The coupling between synaptic vesicles and Ca²⁺ channels determines fast neurotransmitter release. *Neuron*. 2007; 53:563–575. [PubMed: 17296557]
- Wang Y, Okamoto M, Schmitz F, Hofmann K, Südhof TC. Rim is a putative Rab3 effector in regulating synaptic-vesicle fusion. *Nature*. 1997; 388:593–598. [PubMed: 9252191]
- Wang Y, Südhof TC. Genomic definition of RIM proteins: evolutionary amplification of a family of synaptic regulatory proteins. *Genomics*. 2003; 81:126–137. [PubMed: 12620390]
- Wang Y, Sugita S, Südhof TC. The RIM/NIM family of neuronal C₂ domain proteins. Interactions with Rab3 and a new class of Src homology 3 domain proteins. *J Biol Chem*. 2000; 275:20033–20044. [PubMed: 10748113]
- Wölfel M, Lou X, Schneggenburger R. A mechanism intrinsic to the vesicle fusion machinery determines fast and slow transmitter release at a large CNS synapse. *J Neuroscience*. 2007; 27:3198–3210.
- Wu LG, Westenbroek RE, Borst JGG, Catterall WA, Sakmann B. Calcium channel types with distinct presynaptic localization couple differentially to transmitter release in single calyx-type synapses. *J Neurosci*. 1999; 19:726–736. [PubMed: 9880593]
- Zenisek D, Davila V, Wan L, Almers W. Imaging calcium entry sites and ribbon structures in two presynaptic cells. *J Neurosci*. 2003; 23:2538–2548. [PubMed: 12684438]

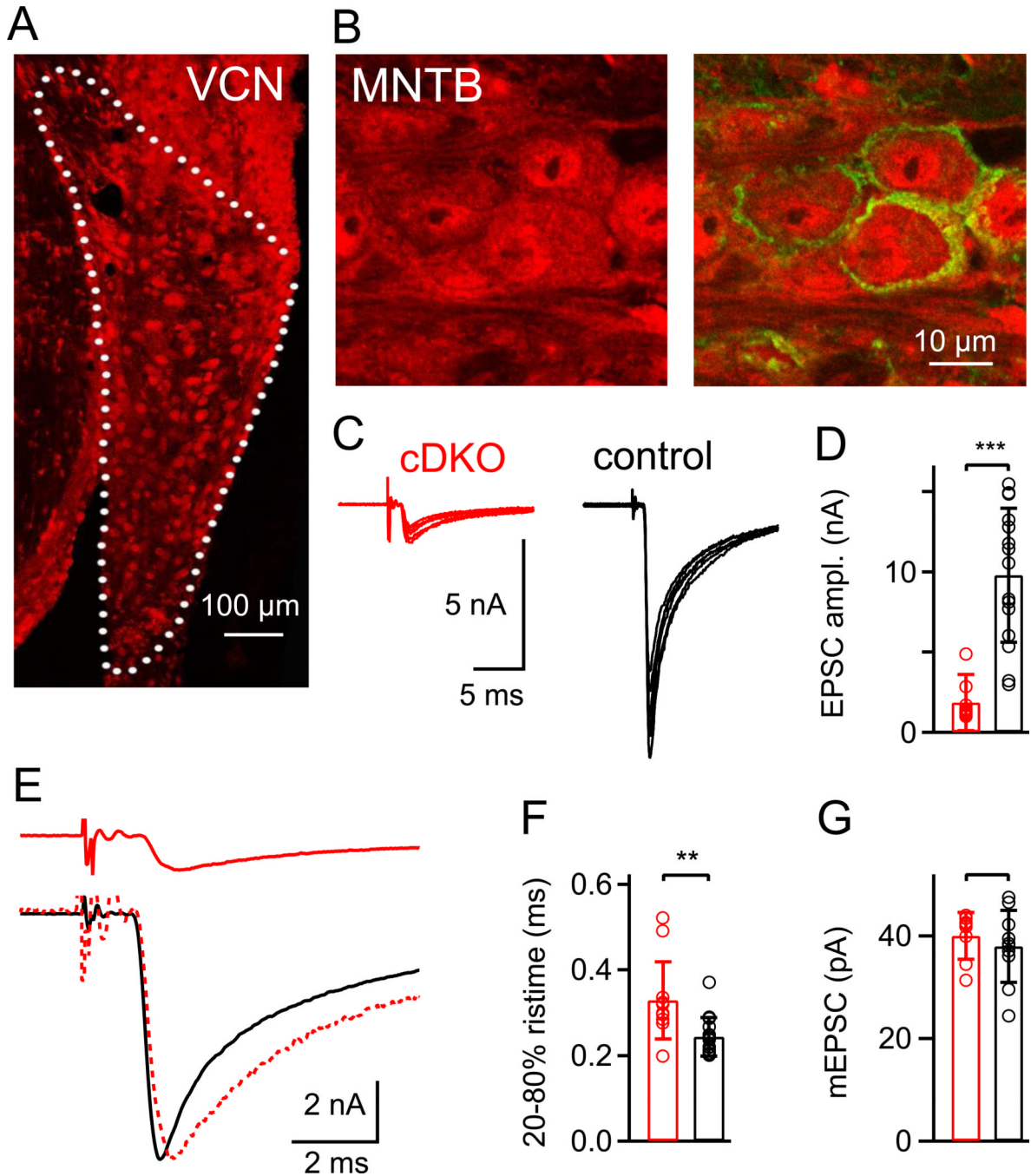


Figure 1. Conditional removal of RIM1/2 in the auditory brainstem leads to strong reduction of transmitter release at the calyx of Held

(A, B) Krox20-driven Cre activity in the VCN (A) and MNTB (B), as revealed by anti-RFP immunohistochemistry (red channel) using a td-RFP reporter mouse. In (A), Cre activity was observed in many VCN neurons, most likely including globular bushy cells which give rise to calyces of Held. Correspondingly, in (B), immunohistochemistry against RFP and against the presynaptic marker Synaptotagmin-2 (green channel; right) shows the presence of RFP in presynaptic calyces of Held, as well as in MNTB principal cells.

(C) Fiber stimulation-evoked EPSCs at the calyx of Held synapse of a Cre-positive, RIM1lox/ Δ , RIM2lox/ Δ mouse (referred to as "cDKO"; *left*), and in a Cre-negative control mouse (*right*). N = 6 consecutive traces are shown for individual cells.

(D) Average and individual values of evoked EPSC amplitudes in RIM1/2 cDKO synapses (n = 12 cells) and in control synapses (n = 15 cells).

(E) Average EPSC traces of the same cells as shown in (C). The lower panel shows an overlay of the EPSC from a control mouse, and a peak-scaled EPSC from a RIM1/2 cDKO mouse, to illustrate a slight slowing of the EPSC rise time in the RIM1/2 cDKO mice.

(F) Average and individual values of the 20 – 80 % rise times. There was a small, but significant (p = 0.0038) slowing in RIM1/2 cDKO mice.

(G) Average and individual values of mEPSC amplitudes in the two genotypes; there was no statistically significant difference (p > 0.05). In this and all subsequent Figures, red and black symbols refer to data from RIM1/2 cDKO synapses and control synapses respectively. Star symbols indicate statistical significance (*, p < 0.05; **, p < 0.01; and ***, p < 0.001); a bracket without star symbol indicates no statistical significance (p > 0.05; Student's t-test). Error bars = SD. See also Figure S1.

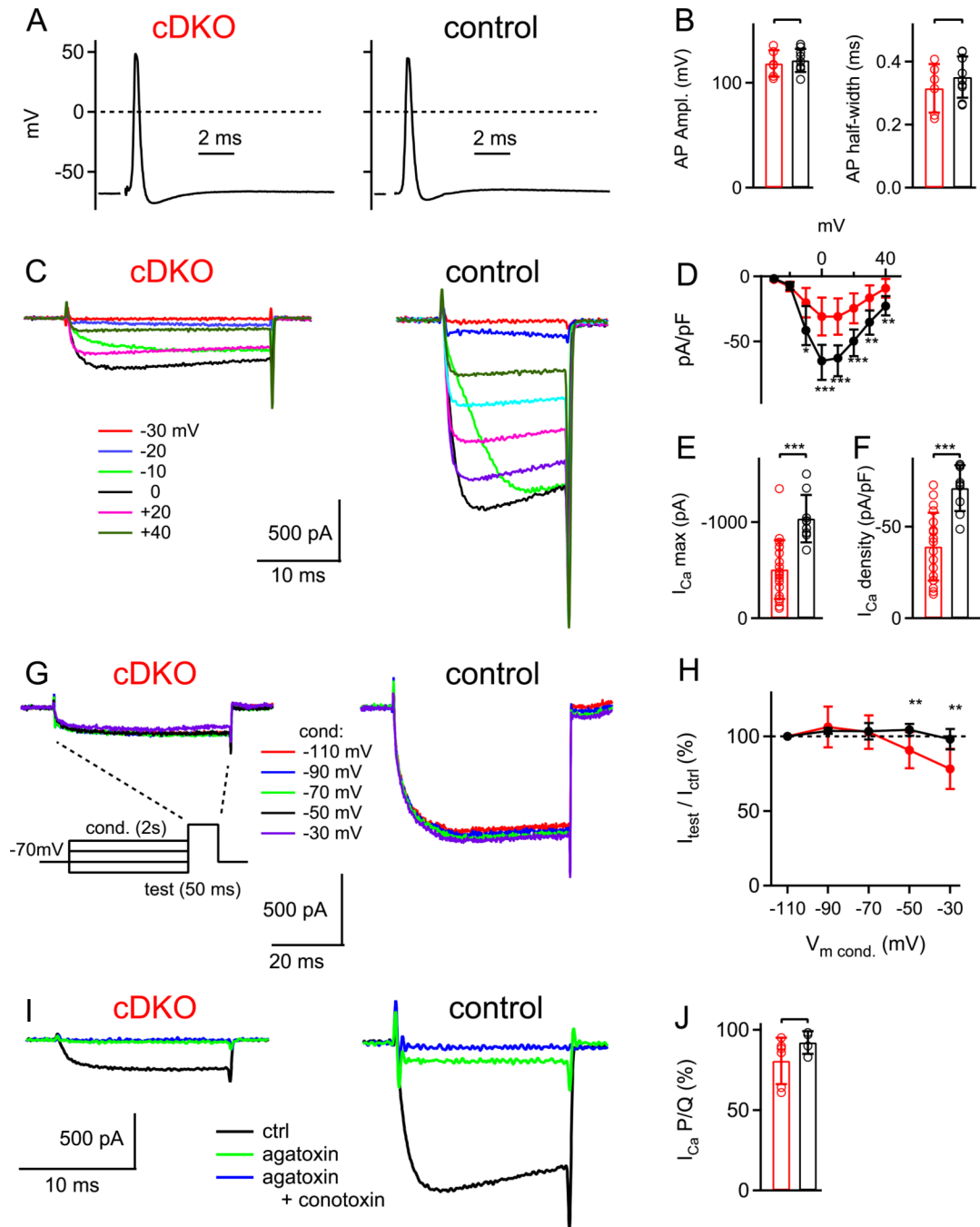


Figure 2. A strong reduction of Ca²⁺ current density in nerve terminals of RIM1/2 cDKO mice (A, B) Presynaptic action potentials (APs) recorded in RIM1/2 cDKO calyces (A, left), and in control calyces (A, right) following afferent fiber stimulation. The average AP amplitudes and AP-halfwidths were unchanged in RIM1/2 cDKO calyces (B). (C) Ca²⁺ currents evoked by voltage-steps to the indicated membrane potentials in a RIM1/2 cDKO calyx (left) and in a control calyx (right). (D) Current-voltage relationship of Ca²⁺ currents normalized by presynaptic membrane capacitance (C_m), averaged for n = 19 RIM1/2 cDKO calyces, and for n = 9 control calyces.

(E, F) Peak Ca^{2+} current amplitude (E) and (C) Ca^{2+} current density following normalization by the presynaptic C_m in RIM1/2 cDKO calyces (red) and in control calyces (black).

(G, H) Presynaptic Ca^{2+} currents in response to a 50 ms test pulse to 0 mV, recorded after conditioning pre-pulses of 2s duration to the indicated membrane potentials. Note that negative pre-pulses did not reveal any significant steady-state inactivation at -70 mV, the holding potential standardly used here. In (H), the percentage of the current measured during the test pulse, relative to the current obtained for the most negative conditioning pulse, is given.

(I, J) Sequential block of presynaptic Ca^{2+} currents by ω -agatoxin-IVa (agatoxin, $0.2 \mu\text{M}$; green trace), and by the subsequent application of ω -conotoxinGVIIa (conotoxin, $3 \mu\text{M}$) in the continuous presence of agatoxin (blue traces). The fraction of the total Ca^{2+} current blocked by agaIVa in the two genotypes was unchanged (J).

Error bars = SD. See also Figure S2.

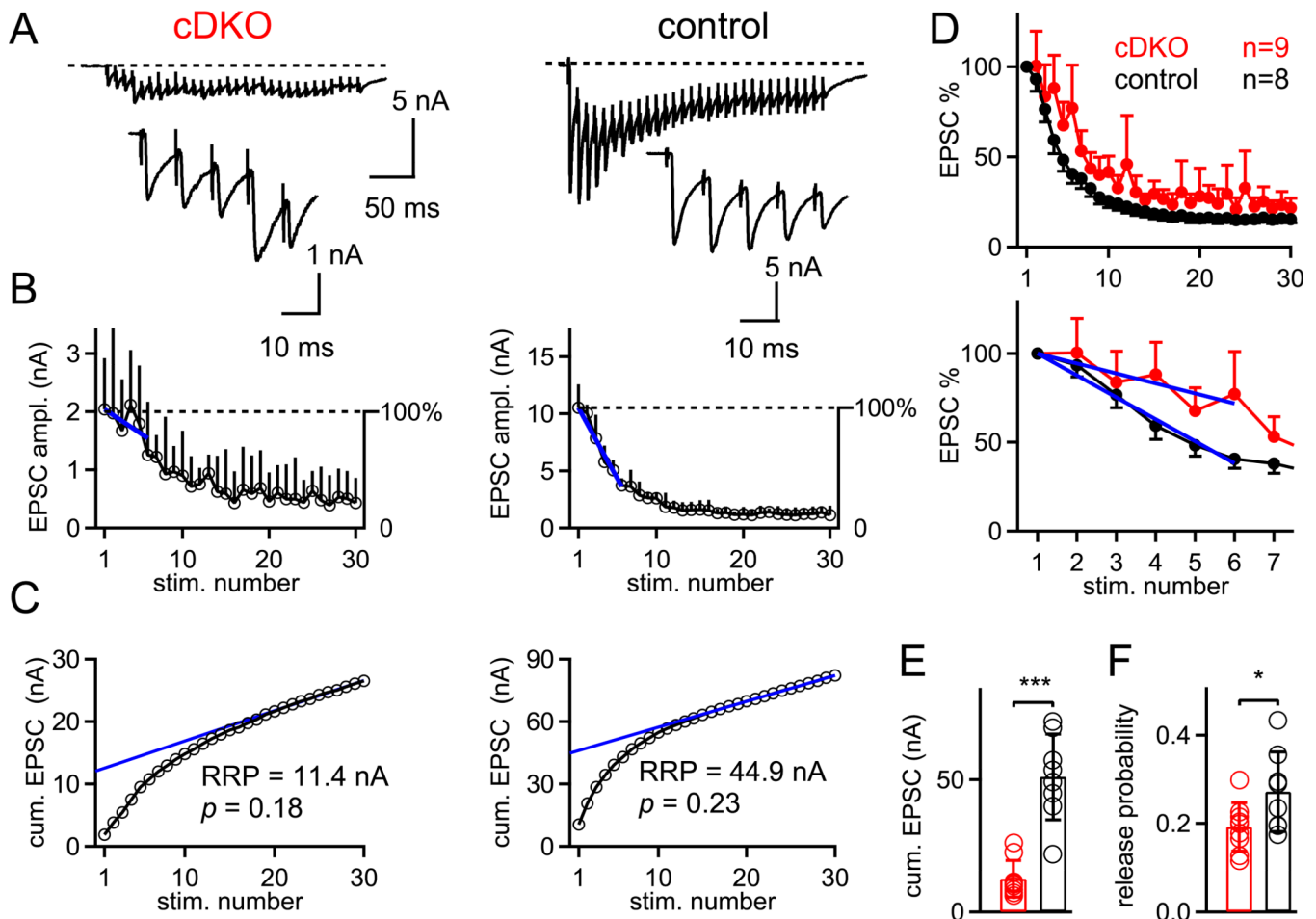


Figure 3. Train stimulation and short term plasticity experiments indicate a reduced pool size and a slightly lowered probability

(A) Example single EPSC traces in response to 100 Hz trains of afferent fiber stimulations in a RIM1/2 cDKO synapse (*left*) and in a control synapse (*right*). The first five EPSCs during the train are shown on increased scales in the insets.

(B) EPSC depression curves averaged over 6 and 7 trials for the same cells as shown in (A). The first six data points following normalization to the first EPSC amplitude (see right-hand y-axis) were fitted with linear functions to quantify the onset of depression in both genotypes (blue fit lines).

(C) Cumulative EPSC amplitude plots for the two cells shown in (A, B). Back-extrapolation to time zero yields the recovery-corrected pool size estimate (Schneeggenburger et al., 1999). Note the much smaller value in the RIM1/2 cDKO neuron (*left*) as compared to the control cell (*right*). Data in A–C are from corresponding recordings.

(D) Plot of the normalized EPSC amplitudes during 100 Hz trains, averaged for all RIM1/2 cDKO (n = 9 cells) and control cells (n = 8). The lower panel shows the data on an expanded time scale, together with the line fits to the average data set (blue lines). Error bars represent S.E.M.

(E, F) Individual and average values of the pool size estimate (E) and of the release probability (F) for RIM1/2 cDKO (*red*) and control synapses (*black*). Error bars = SD (except panel D; = SEM).

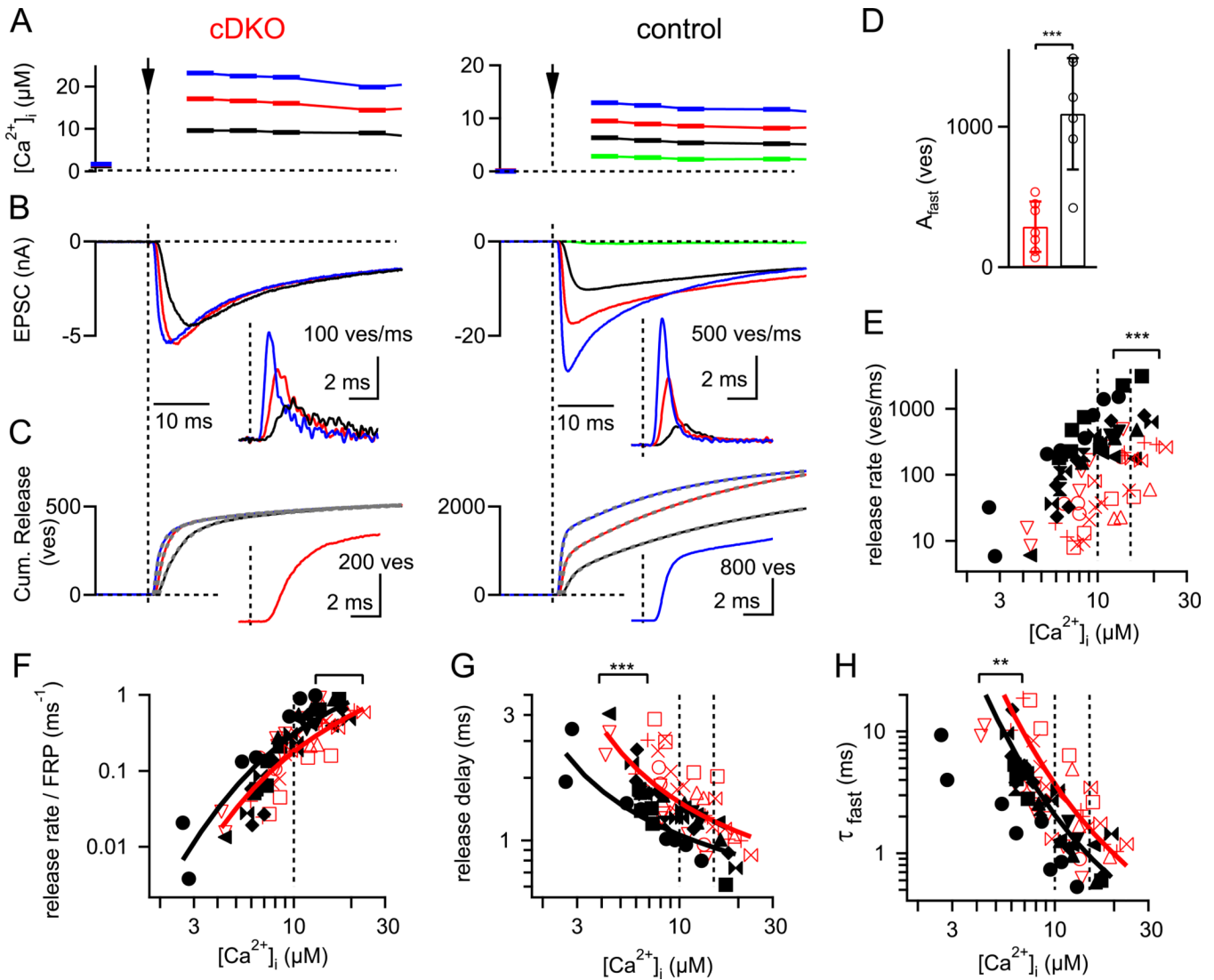


Figure 4. Presynaptic Ca^{2+} uncaging reveals a smaller readily-releasable pool and a decrease in the intrinsic Ca^{2+} sensitivity

(A – C) Ca^{2+} uncaging - evoked elevation of presynaptic $[\text{Ca}^{2+}]_i$ (A), postsynaptic EPSCs (B), and cumulative transmitter release (C) in a RIM1/2 cDKO (left) and control synapse (right). The insets in (B) show the transmitter release rates. Note the much smaller Ca^{2+} uncaging - evoked EPSCs in the RIM1/2 cDKO synapse, which indicate a strongly reduced readily-releasable pool. The cumulative release traces in (C) were best fitted with double-exponential, or double-exponential plus line functions (Dashed grey traces; see Experimental Procedures). The insets in (C) show cumulative release traces in response to roughly similar $[\text{Ca}^{2+}]_i$ steps ($\sim 15 \mu\text{M}$) on an expanded time-scale, to illustrate the slowed rise and longer delay in RIM1/2 cDKO synapses.

(D) The number of fast-released vesicles for $[\text{Ca}^{2+}]_i$ steps in the range of 10 – 15 μM , as obtained by the amplitude parameter of the fast fit component of double-exponential fits to the cumulative release traces (see C).

(E) Plot of the peak transmitter release rates as a function of the $[\text{Ca}^{2+}]_i$ step amplitude for both genotypes. The statistical significance between the data sets was determined by ANCOVA ($p < 0.001$).

(F – H) Pool-normalized peak release rate (F), release delays (G) and the time constant of the fast release component (H), plotted against the amplitude of the $[Ca^{2+}]_i$ steps. Note the significantly slower release delays (G) ($p < 0.001$; ANCOVA) and fast release time constants (H) ($p < 0.01$; ANCOVA). The five site model of Ca^{2+} binding and vesicle fusion (Schneggenburger and Neher, 2000) was globally fitted to all three data sets (F, G, H), for each genotype. The resulting fit parameters indicate that slowed Ca^{2+} - binding (decreased on-rate, and slightly decreased off-rate; see Experimental Procedures for parameters) could describe the data in the RIM1/2 cDKO synapses. Error bars = SD.

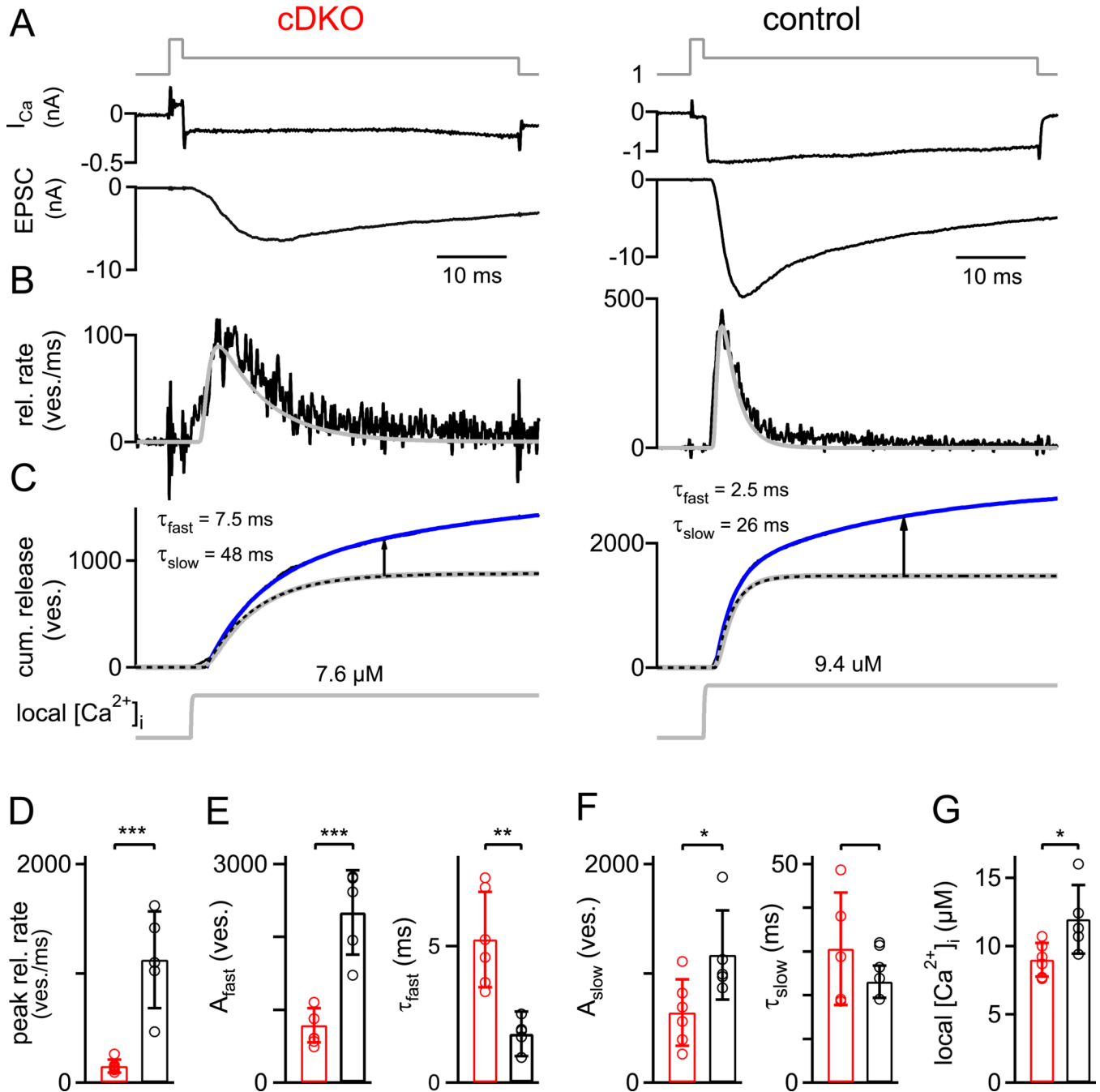


Figure 5. Paired pre- and postsynaptic recordings show a deficit in Ca^{2+} channel - release coupling in addition to the strongly decreased pool size
 (A–C) Transmitter release in response to prolonged presynaptic depolarizations. Ca^{2+} currents and EPSCs (A, upper and lower panel), release rates (B), traces of cumulative release (C, upper), and the back-calculated local $[Ca^{2+}]_i$ signal (C, lower) are shown. The double-exponential (best) fit of the cumulative release traces is overlaid as a blue line over the data (black lines, not visible). The dotted black traces in (C) are the fast components of the double exponential fits. The grey traces overlaid over the transmitter release rates (B) and the fast release component (C) are the predicted release rates determined by the back-calculation approach using the five-site model of Ca^{2+} binding and vesicle fusion

(Schneggenburger and Neher, 2000), which effectively models the fast release component. The arrows show the estimated amplitude of the slow release component at a time of 30 ms.

(D) Average peak release rates of both genotypes.

(E) Estimate of FRP obtained from the amplitude parameter of the fast release component (*left*, in number of vesicles), and time-constant of the fast release component (*right*), for both genotypes.

(F) Number of slowly-released vesicles (*left*) and slow release time-constant (*right*), for both genotypes.

(G) Average and individual values of the amplitude of the back-calculated local $[Ca^{2+}]_i$ as shown in C (lower panel; grey traces). Note the slightly, but significantly ($p = 0.03$) smaller local $[Ca^{2+}]_i$ that was back-calculated for the RIM1/2 cDKO synapses. Error bars = SD. See also Figure S3.

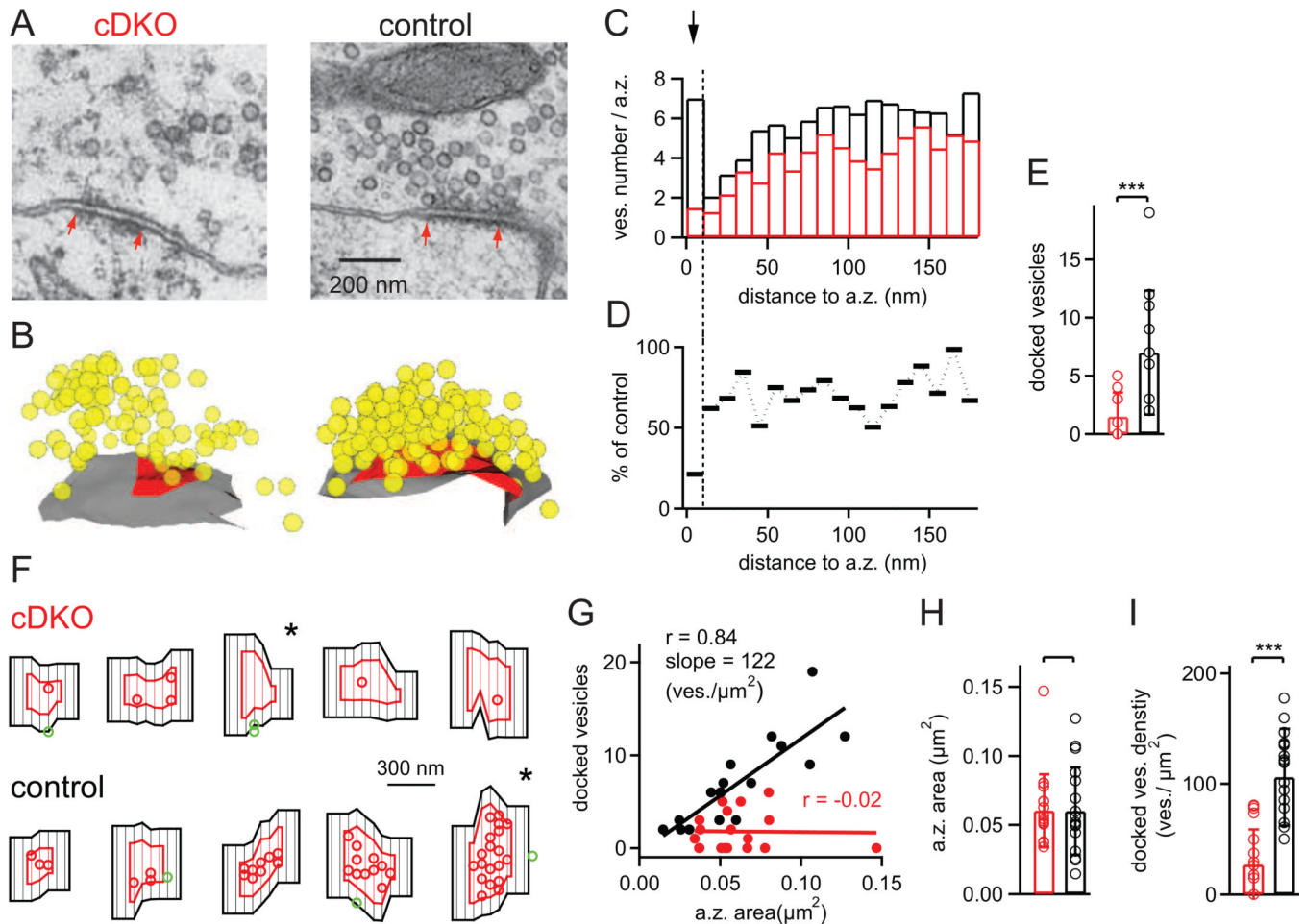


Figure 6. RIM1/2 docks vesicles to the presynaptic active zone

(A, B) Representative single EM images of calyceal active zones, and three-dimensional reconstructions of the corresponding active zones from a RIM1/2 cDKO mouse (*left*), and from a control mouse (*right*) from the same P11 litter. Red arrows in (A) indicate the extent of the postsynaptic density, which was used to measure the active zone sizes. In (B), vesicles are shown in yellow; active zone membrane is indicated in red.

(C) Average histogram of vesicle numbers located at different distances to the active zone; bin width = 10 nm ($n = 18$ and $n = 17$ active zones for RIM1/2 cDKO and control mice respectively). Note that in control synapses, the bin at the shortest distance shows a peak which likely represents the pool of docked vesicles; this peak was strongly reduced in RIM1/2 cDKO synapses (see arrow).

(D) Percentage value of average vesicle numbers shown in (C), calculated as RIM1/2 cDKO values relative to control. Note the much stronger reduction for the membrane-nearest bin (10 nm and less), indicating a strong vesicle docking deficit in RIM1/2 cDKO mice.

(E) Average number of docked vesicles, defined as vesicles located within 10 nm from the active zone membrane. Note the significant decrease in the number of docked vesicles in RIM1/2 cDKO synapses ($p < 0.001$). Also note that due to integer numbers, not all data points are visible ($n = 18$ and 17 for RIM1/2 cDKO and control, respectively).

(F) Examples of flat surface rendered active zones (*red*) and adjacent membrane (*black*) within 100 nm distance from the active zone boarder. Docked vesicles within the active zone and outside are shown as red and green circles, respectively. Five examples for RIM1/2 cDKO (upper row) and for control active zones are shown, ordered according to increasing

active zone surface. Note the strongly reduced density of docked vesicles in RIM1/2 cDKO synapses, and the only small number of "outlier" vesicles adjacent to the active zone in both genotypes. The star symbols mark the example active zones shown in (A, B).

(G) Plot of the number of docked vesicles versus active zone area. Linear regression showed a good correlation and near-linear relationship in the control data with the indicated regression coefficient and slope. In the RIM1/2 cDKO, the data was dominated by a low number of docked vesicles irrespective of active zone size.

(H, I) Average and individual values of active zone area (H), and docked vesicle density per μm^2 of active zone membrane (I). The latter values were obtained by normalizing the docked vesicle numbers (E) to the corresponding active zone area (H).

Error bars = SD. See also Table S1.